J Musculoskelet Neuronal Interact 2016; 16(2):122-134

Journal of Musculoskeletal and Neuronal Interactions JMNI

Original Article

Severe muscle trauma triggers heightened and prolonged local musculoskeletal inflammation and impairs adjacent tibia fracture healing

B.J. Hurtgen[1†], C.L. Ward[1], K. Garg[1], B.E. Pollot[1], S.M. Goldman[1], T.O. McKinley[2], J.C. Wenke[1], B.T. Corona[1]

[1]Extremity Trauma and Regenerative Medicine Task Area, US Army Institute of Surgical Research, Fort Sam Houston, TX; [2]Department of Orthopaedic Surgery, Indiana University School of Medicine, Indianapolis, IN

Abstract

Objectives: Complicated fracture healing is often associated with the severity of surrounding muscle tissue trauma. Since inflammation is a primary determinant of musculoskeletal health and regeneration, it is plausible that delayed healing and non-unions are partly caused by compounding local inflammation in response to concomitant muscle trauma. **Methods and results:** To investigate this possibility, a Lewis rat open fracture model [tibia osteotomy with adjacent tibialis anterior (TA) muscle volumetric muscle loss (VML) injury] was interrogated. We observed that VML injury impaired tibia healing, as indicated by diminished mechanical strength and decreased mineralized bone within the fracture callus, as well as continued presence of cartilage instead of woven bone 28 days post-injury. The VML injured muscle presented innate and adaptive immune responses that were atypical of canonical muscle injury healing. Additionally, the VML injury resulted in a perturbation of the inflammatory phase of fracture healing, as indicated by elevations of $CD3^+$ lymphocytes and $CD68^+$ macrophages in the fracture callus at 3 and 14d post-injury, respectively. **Conclusions:** These data indicate that heightened and sustained innate and adaptive immune responses to traumatized muscle are associated with impaired fracture healing and may be targeted for the prevention of delayed and non-union following musculoskeletal trauma.

Keywords: Skeletal Muscle Injury, Volumetric Muscle Loss, Trauma, Musculoskeletal, Inflammation, Innate, Adaptive, Immune Response, Composite Injury

Introduction

Musculoskeletal injuries are highly prevalent in civilian and military trauma and can impart permanent disability[1,2]. A volumetric loss of muscle tissue adjacent to fractured bone is frequently encountered (e.g., type IIIa/b open fracture). Volumetric muscle loss (VML) injuries are irrecoverable in humans and animal models- owing to the complete loss of crucial elements for skeletal muscle regeneration. Since there are no therapies clinically available that can regenerate the lost musculature, VML is often untreated and considered part of the natural sequelae of trauma. As a result, VML injury manifests a permanent loss of contractile tissue, extensive fibrosis, and a chronic loss of function[3-7], which may directly lead to disability in open fracture patients[8] that may progressively worsen with time[9].

While VML injuries result in chronic reduction of limb functional capacity, acutely after trauma these severe muscle injuries may also impair healing of adjacent fractured bone. This is exemplified by the clinical grading of open fractures whereby severe fracture with predictably worse healing outcomes are predicated on the extent of surrounding soft tissue comorbidity[10]. In some of these cases (e.g., type IIIb), free or

The authors have no conflict of interest. The opinions or assertions contained herein are the private views of the authors and are not to be construed as official or as reflecting the views of the Department of the Army or the Department of Defense.

Corresponding author: Benjamin T. Corona, Extremity Trauma and Regenerative Medicine Task Area, US Army Institute of Surgical Research, 3698 Chambers Pass, BHT1, Fort Sam Houston, TX 78234
E-mail: benjamin.t.corona.vol@mail.mil • corona.benjamin.t@gmail.com

Edited by: F. Rauch
Accepted 4 April 2016

rotational muscle flaps are transferred to the site of VML, signifying the importance of restoring muscle-bone interactions to fracture healing. In support of clinical observations, animal models have unequivocally demonstrated that the loss of adjacent musculature impairs fracture healing. For instance, a series of studies performed in a rat self-healing tibia fracture model demonstrated that tibialis anterior (TA) muscle ablation delayed recovery of tibia mechanical properties[11-13]. Additionally, in a rat femur critical size defect model, adjacent quadriceps VML (~10% loss of muscle) impaired rhBMP-2 mediated fracture healing[14]. Lastly, in a mouse simple fracture model TA muscle dissection and further isolation of the fracture site from the posterior musculature impaired fracture healing[15]. All told, it is clear that the traumatic or surgical loss of surrounding musculature has a deleterious effect on fracture healing.

Mechanisms bridging VML with compromised bone healing intuitively involve compromised regional blood flow, but also may be affected by localized VML-associated effects on fracture inflammation. Dysregulated inflammation is associated with diminished bone strength and impaired fracture healing. For example, disease conditions that present chronic systemic inflammation, such as diabetes mellitus, inflammatory bowel syndrome, and rheumatoid arthritis are associated with increased susceptibility to fracture[16-19]. Moreover, elevated systemic inflammation following polytrauma (e.g., fracture concomitant with blunt chest trauma) has been associated with delayed fractured healing[20,21]. Notably, there is also evidence that local muscle inflammation may also mediate fracture healing. In a mouse model of Duchenne muscular dystrophy, dystrophin deficiency results in chronic muscle inflammation, diminished bone strength, and impaired fracture healing[22-24]. To date very little is understood of the immune response to traumatic VML injury and its potential role in local musculoskeletal healing. Therefore, the purpose of this study was to characterize the immune response to VML injury and to assess whether concomitant VML altered macrophage or T-lymphocyte cellular infiltration within an adjacent diaphyseal fracture in a rat muscle-bone composite injury model that presents VML-dependent delayed fracture healing.

Materials and methods

Surgical protocol

All animal procedures were approved by the Institutional Animal Care and Use Committee and were conducted in compliance with the Animal Welfare Act and in accordance with the principles of the Guide for the Care and Use of Laboratory Animals. Inbred male Lewis rats (350-400 g) were housed in a specific-pathogen-free animal facility at the US Army Institute of Surgical Research. Rats underwent an osteotomy (OST) and, to create an open fracture in selected groups, a volumetric muscle loss injury (OST+VML) as described elsewhere[5]. Briefly, rats were anesthetized and a longitudinal incision was made along the lateral aspect of the leg and the skin and fascia covering the tibialis anterior (TA) muscle were bluntly separated from the underlying musculature. The tissue covering the middle third of the tibia was separated bluntly from the bone. An osteotomy was performed approximately 5 mm proximal to the tibia-fibula junction and stabilized with a 1.25 mm Kirschner pin inserted in the medullary cavity from the tibial plateau. To surgically create a volumetric muscle loss, the TA muscle and underlying extensor digitorum longus (EDL) muscle were separated using blunt dissection and a punch biopsy (6 mm) was executed through the middle third of the TA muscle and the tissue was removed, as we have previously reported[3,5]. Controls consisted of either naïve housing controls or sham surgery animals that underwent all surgical procedures except osteotomy or VML (n=3-6 per group).

Micro-computed tomography

Microcomputed tomography (μCT) scans (Viva-CT40, Scanco Medical) were performed on a set of rat tibias at 28d post-injury. Osteotomy regions were scanned at medium resolution with a 21 μm voxel size at a voltage of 55 kVp and a current of 145 μA. A volume of interest of 400 slices was analyzed (~8.4 mm) with a centralized osteotomy site. Bone and callus were segmented by applying a threshold corresponding to 455 mg hydroxyapatite/cm^3 and a low-pass Gaussian filter (sigma=1.2, support=1.0) was applied to suppress noise. Contours were first drawn around the entire specimen to obtain a total volume and then drawn around the cortical bone to obtain bone (original) volume. Callus volume was calculated by subtracting bone (original) volume from total volume, expressed as mm^3.

Three-point bending mechanical testing

Three-point bending was performed on a set of rat tibias at 28d post-injury. For these samples, after harvesting, bones were stripped of muscles and adjoined fibulas, and placed in phosphate buffered saline (PBS). To eliminate any equipment variability, all samples were frozen at -80°C until testing could be performed at one time. Prior to mechanical testing, samples were thawed in a water bath at 37°C for approximately 1 hour. Briefly, tibias were placed in a materials bending system (Lloyd LRX) along the sagittal plane, with the medial (flat) portion of the tibia resting on the lower points, separated by 20 mm. Samples were deflected by lowering the apparatus at the midpoint of the lateral side of the bone. Samples were loaded at a constant speed of 2 mm/min until failure. Tibias from contralateral legs (without injury) were tested as controls. Load-deflection curves were used to obtain maximum load (N) and stiffness (N/mm).

TA muscle histology

Comparative histopathology and immunofluorescence staining methods were conducted with tissue sections from the middle third of the TA muscle that comprised the VML defect as well as bone tissue. TA muscle tissue isolation and

Table 1. Nucleotide sequence for primers used for quantitative RT-PCR.

	Forward sequence	Reverse sequence	Amplicon length, bp
ARG1	5'-GTGAAGAACCCACGGTCTGT-3'	5'-GTGAGCATCCACCCAAATG-3'	180
CCR7	5'-GCTCTCCTGGTCATTTTCCA-3'	5'-AAGCACACCGACTCATACAGG-3'	107
CD163	5'-TCATTTCGAAGAAGCCCAAG-3'	5'-CTCCGTGTTTCACTTCCACA-3'	101
iNOS	5'-ACTGTGTGCCTGGAGGTTCT-3'	5'-GACACAAGGCCTCCAACCT-3'	193
MRC1	5'-CAAAACAAAGGGACGTTTCG-3'	5'-CCTGCCACTCCAGTTTTCAT-3'	116
18S	5'-GGCCCGAAGCGTTTACTT-3'	5'-ACCTCTAGCGGCGCAATAC-3'	173

freezing was performed as described previously[3,5]. Tissue sections (10 µm thickness) were stained with hematoxylin and eosin (H&E) by standard procedure or probed for laminin, CD68, and nuclei (DAPI) using previously reported methodology[3,5]. Composite images of the complete TA muscle were acquired using Axio Scan.Z1 microscope (Zeiss) and ZEN imaging software (Zeiss). Sections were also examined by brightfield and fluorescence microscopy (Olympus IX71) and images of muscle tissue were acquired and analyzed using cellSens Standard software (Ver 1.4.1, Olympus).

Real-time PCR

RNA was extracted from the muscle defect as previously described[3]. Briefly, the defect was excised and flash frozen in liquid nitrogen. Approximately 50 mg of muscle tissue was removed and homogenized. RNA was isolated using TRIzol and purified using an RNeasy Mini Kit (Qiagen) per manufacturer's protocol. RNA was converted into complementary DNA (cDNA) using RT2 First Strand Kit (Qiagen). A vendor-designed RT^2 Profiler PCR array (PARN052Z, SABiosciences) with was employed to examine rat innate and adaptive immune responses. Custom designed primers (Sigma-Aldrich) with the sequences presented in Table 1 were used for select genes. A C1000 Touch Thermo Cycler equipped with a CFX96 Real-Time System (BioRad) was used to determine gene expression. Data analysis was carried out either with the RT^2 Profiler PCR Array Data Analysis version 3.5 or expression levels for each mRNA transcript were determined by the $2^{-\Delta\Delta CT}$ method. Gene expression in OST+VML muscle tissue was relative to expression in contralateral control muscle tissue and normalized to reference gene, *Rplp1* or *Rn18s* (n=3-6 per group).

Isolation of cellular infiltrates from muscle defect

Cells were isolated from complete TA muscle defect by enzymatic digestion. The defect was surgically isolated and the mass was determined. In 1.5 ml tubes, tissue was incubated with 1% collagenase type II and 2.4 U/mL of dispase dissolved in phosphate buffered saline (PBS) plus 2.5 mM calcium chloride for 90 minutes at 37°C. Following enzymatic digestion, cells were further released in a tissue culture plate containing RPMI 1640 media plus L-glutamine and 5% heat-inactivated fetal bovine serum (FBS) by gentle mechanical disruption using the back of a sterile 3-ml syringe plunger and filtered through a cell strainer (70 µm pore size). Erythrocytes were lysed with ammonium-chloride-potassium (ACK) lysing buffer and cells were pelleted by centrifugation at 1500 RPM for 10 min, 4°C. Cells were subsequently filtered through a cell strainer (40 µm pore size), washed, and resuspended in wash buffer that consisted of PBS containing 0.5% FBS and 0.1% sodium azide. Viable cells were visualized by trypan blue exclusion and quantified by light microscopy using a hemocytometer.

Table 2. Antibodies used for flow cytometry.

Antigen	Antibody Clone	Vendor
CD3	IF4	BD Pharmingen
CD4	OX-35	BD Pharmingen
CD8α	OX-8	BD Pharmingen
CD11b	WT.5	BD Pharmingen
CD45	OX-1	BD Pharmingen
CD68	ED1	AbD Serotec
CD86	24F	BD Pharmingen
CD163	ED2	AbD Serotec

Quantification of cellular infiltrates in muscle defect

Approximately 2-4 x 10^5 cells were incubated with anti-CD32 antibody to block Fc receptors. Cells were washed and then labeled for 30 min with one of two cocktails of fluorochrome-conjugated monoclonal antibodies described in Table 2 to identify myeloid cells or T lymphocytes. The myeloid cell cocktail included anti-CD45, anti-CD11b, anti-CD86, and anti-CD163. The T lymphocyte cell cocktail consisted of anti-CD3, anti-CD4, and anti-CD8α. Labeled cells were washed twice and fixed with 1% paraformaldehyde. Labeled cells (100,000 or 200,000 cells per myeloid or lymphoid samples, respectively) were enumerated by fluorescence-activated cells sorting (FACS) using a MACSQuant flow cytometer (Miltenyi Biotec). Data were analyzed using MACSQuantify software (Miltenyi Biotec). Gating strategies to identify cellu-

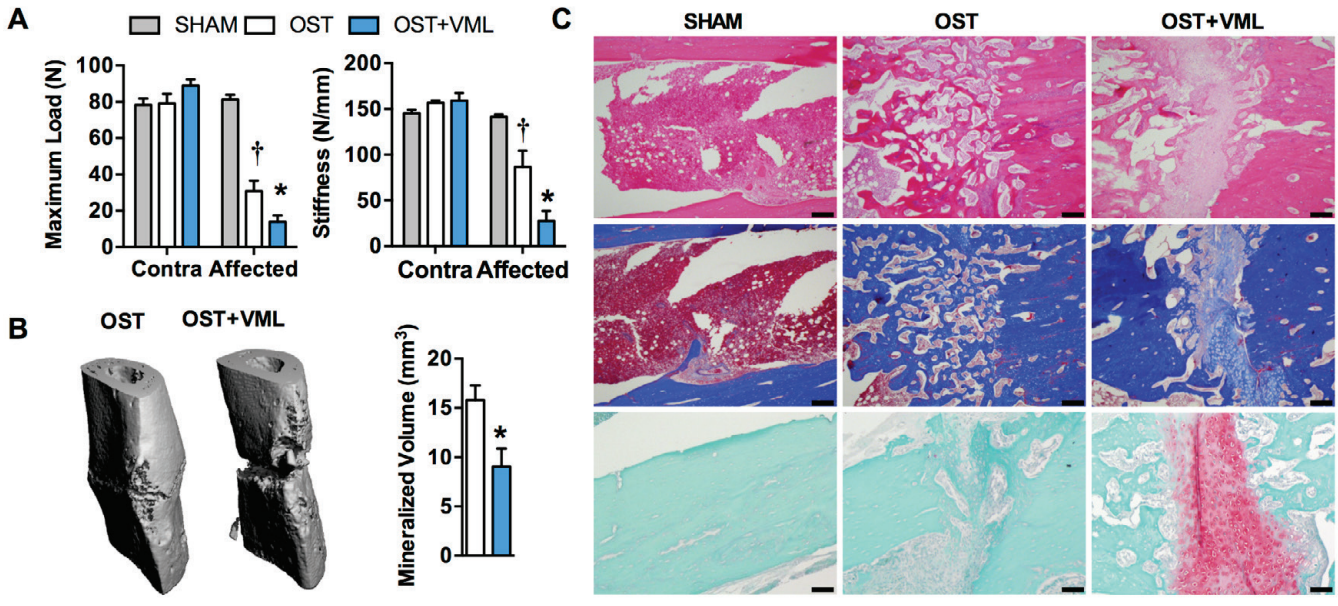

Figure 1. Traumatized muscle impairs bone healing after open fracture. Three-point bending mechanical testing and μCT imaging of tibiae were performed at 28 days post-injury. A) Contralateral tibia maximum load and stiffness were similar among groups and no significant difference was observed between contralateral and affected tibia of the SHAM group. Significant differences were detected among affected limb groups. † affected OST vs. contralateral OST & affected SHAM; * affected OST+VML vs. contralateral OST+VML & affected SHAM and OST groups (p-values <0.05). B) Representative μCT images of OST and OST+VML tibiae are presented from which callus volume was calculated; * $p<0.05$. Values are means ± SEM; n=4 – 6 per group. C) Histology of tibia of affected limb. Top, middle, and bottom rows: H&E, Masson's Trichrome, and Safrinin O. Scale bars = 200 μm.

lar populations included the following: $CD45^+CD11b^+$ myeloid cells, $CD45^+CD11b^+CD86^+$ M1-like cells, $CD45^+CD11b^+CD163^+$ M2-like cells, $CD3^+CD4^+$, and $CD3^+CD8\alpha^+$ T lymphocytes. $CD45^+CD11b^+$ cells were confirmed as >99% $CD68^+$ in a separate control experiment. To determine the cell numbers of each myeloid cell population, the numbers of hematopoietic cells were first determined by multiplying the percentage of $CD45^+$ cells by the total number of viable cells recovered from the respective defect. The cell numbers of myeloid cells were then determined by multiplying the percentage of $CD11b^+$ cells by the total number of calculated hematopoietic cells. The cell numbers of M1- or M2-like cell populations were then determined by multiplying their percentage by the total number of calculated myeloid cells. The cell numbers of $CD4^+$ and $CD8^+$ lymphocyte populations were determined by first multiplying the percentage of $CD3^+$ cells by the total number of viable cells followed by multiplying this number by the percentage of $CD4^+$ or $CD8\alpha^+$ cells. All cell numbers were normalized per gram of excised muscle tissue.

Tibia histology

Histology was conducted on a set of rat tibiae at 28d post-injury. Bones were harvested from rats and fixed in 10% neutral buffered formalin for a minimum of 7 days. Bones were then rinsed in water and decalcified for 7d in a formic acid bone decalcifier (Immunocal, Decal Chemical Corp, Tallman NY). Samples were processed in paraffin and embedded in a longitudinal orientation. Bone was cut in 8 μm sections, deparafinized, and was stained with hematoxylin and eosin (H&E), trichrome, and safranin O by standard procedure. Sections were also stained with CD68 or CD3 primary antibodies with biotinylated IgG secondary antibody. Detection using 3,3'-diaminobenzidine (DAB) was performed to visualize the stain. For analysis, 4 images (10x magnification) were taken in the osteotomy and callus region (not including the marrow cavity) of each sample. Three samples were analyzed for each group at 3 and 14d. Images were converted to 8bit black and white images (ImageJ, NIH) and a threshold was set to include positively stained cells (evident with brown chromogen staining). Thresholds were applied to all images within a batch and ImageJ software was used to count positive cells.

Statistics

Dependent variables were analyzed using ANOVA or independent samples t-tests. Post-hoc means comparisons testing was performed when a significant ANOVA was observed. Alpha was set at 0.05. Statistical testing was performed with Prism 6 for Mac (Graphpad, La Jolla, CA, USA).

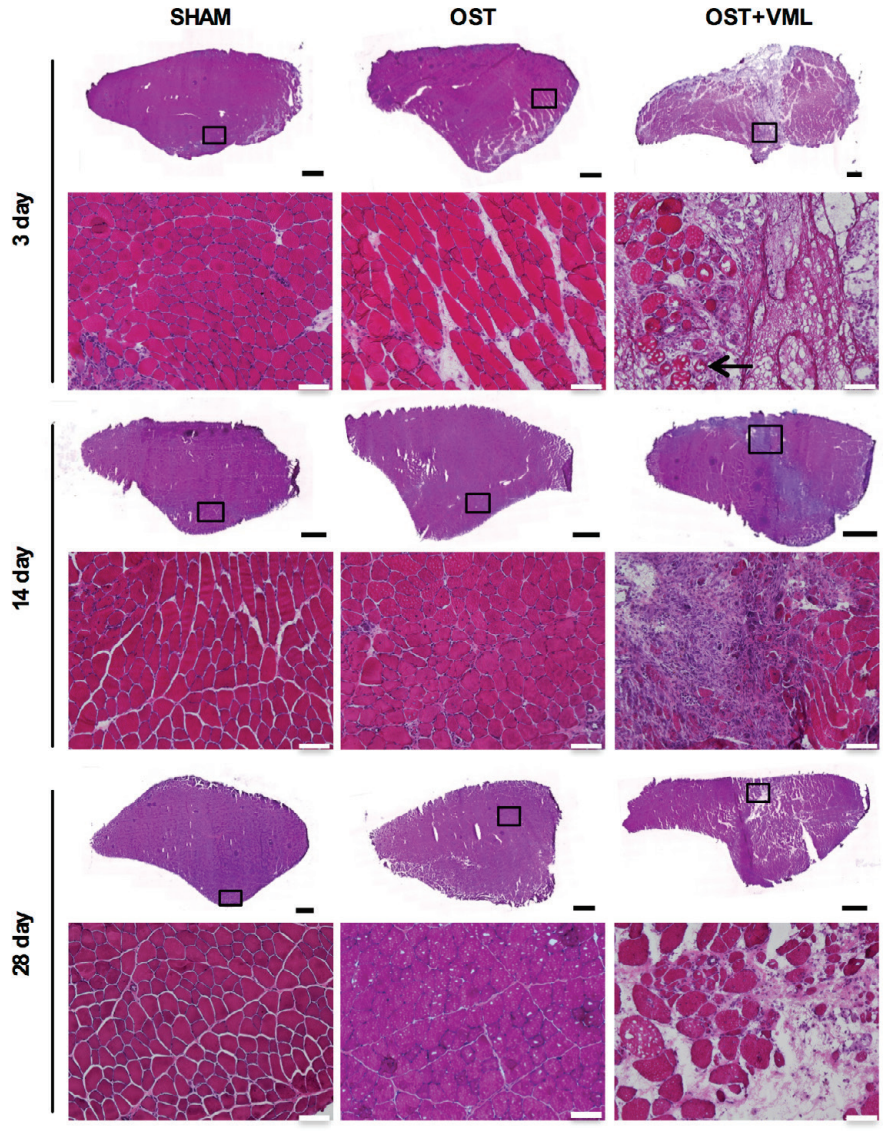

Figure 2. VML injury leads to increased cellular infiltration to TA muscle. The TA muscle was isolated at 3, 14, and 28 days post-trauma from SHAM, OST, and OST+VML groups. Tissue sections were stained with H&E. Representative images of TA cross-sections and magnified regions (inset black boxes) displaying overall muscle morphology and cellular recruitment were collected. Black arrows denote degenerating muscle fibers. n=4 per group. Black scale bars=1.0 mm and white scale bars=100 μm.

Results

Severe muscle trauma impairs adjacent bone healing

A rat model of bone-muscle composite injury was interrogated, in which the tibia and the overlying tibialis anterior (TA) muscle underwent osteotomy (OST) and VML injury, respectively[5]. Tibia mechanical strength and stiffness (Figure 1a) and bone volume within the fracture callus (Figure 1B) were reduced 28d post-injury in the presence of adjacent TA muscle VML injury. These findings are corroborated histologically by the heightened presence of cartilage instead of woven bone within the fracture callus 28d post-injury (Figure 1c). Overall, these findings indicate concomitant VML injury impairs adjacent tibia healing.

Severe muscle trauma invokes cellular recruitment

As an initial assessment of immune cell infiltration following VML injury, H&E sections of TA muscles were analyzed (Figure 2). TA muscles from OST groups presented modest cellular infiltration and muscle fiber damage that was resolved by 28d post-injury following stereotypical muscle fiber repair[25,26]. Consistent with previous observations of iso-

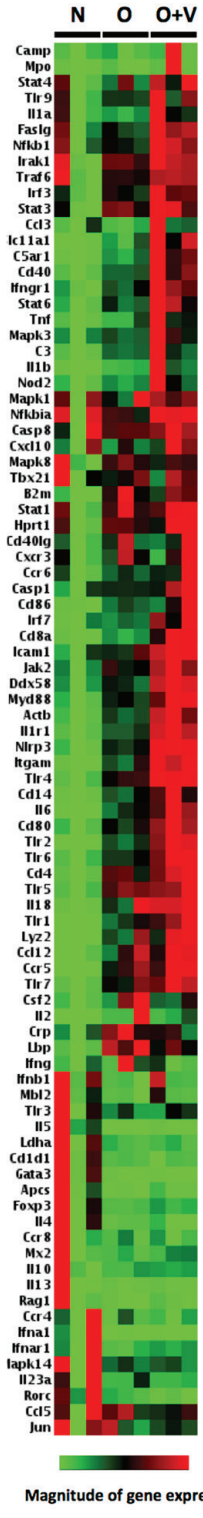

Figure 3. Increased expression of genes involved in innate and adaptive immune responses following complex musculoskeletal injury. Clustergram analysis displaying gene expression values in TA muscle tissue from naïve, OST, and OST+VML groups 3 d post-trauma as determined by PCR array (PARN-052Z, SABiosciences). n=3 per group. Magnitude of gene expression is depicted by color. Green represents reduced expression, black represents no change, and red represents increased expression according to the average value of the gene in all samples.

lated VML injury[3,27], OST+VML presented extensive cellular infiltration to the muscle defect 14d post-injury, which was partly reduced 28d post-injury.

Increased expression of genes involved in innate and adaptive immune responses in skeletal muscle following composite injury

The immune response in VML injured muscle was further compared to the modest, resolvable TA muscle fiber damage in OST groups 3d post-injury by PCR array. Clustergram analysis revealed that VML injury broadly upregulates expression of genes involved in innate and adaptive immune responses (Figure 3). More specifically, expression of genes involved in the acute phase response, inflammasome, pattern recognition receptors (PRRs), downstream components of intracellular signaling pathways, effector functions including cytokine/chemokine production, and other innate genes trended towards or were significantly up-regulated following OST+VML injury (Table 3). Moreover, gene expression of T-cell markers and adhesion molecules involved in T-cell-antigen presenting cell (APC) interaction trended towards or were significantly greater after OST+VML than OST-only.

Heightened innate immune response consisting of a mixed M1/M2 macrophage phenotype is triggered in muscle tissue adjacent to a fracture

Initial immunofluorescence staining of TA muscle sections revealed increased recruitment of $CD68^+$ macrophages at 3 and 14 days post-trauma following OST+VML (Figure 4A). To accurately quantitate cellular recruitment over a longer period of time, flow cytometric analysis of cells isolated from the middle third of the TA muscle adjacent to the tibia osteotomy was conducted through 28d post-trauma. Cells were initially gated for $CD45^+$ hematopoietic cells followed by $CD11b^+$ myeloid cells that were determined to be $CD68^+$ at 3d (data not shown) and either $CD86^+$ M1-like or $CD163^+$ M2-like macrophages (Fig 4B). Overall, the majority of the cells recruited following open fracture were $CD45^+CD11b^+$ myeloid cells (92.30 +/-0.41%). At 3, 14, and 28d post-injury, OST+VML injured muscles had 3.86, 6.77, and 6.50 times greater $CD45^+CD11b^+$ cells, respectively, than OST muscles (Figure 4C). The cell numbers of M1-like ($CD11b^+CD86^+$) to M2-like ($CD11b^+CD163^+$) macrophages in OST+VML versus OST groups were elevated through 28d (Figures 1D&E). Ratios (mean±SEM) of M1/M2 cell numbers were similar at 3d (0.86±0.08 vs. 0.85±0.12; p=0.97), but were higher at 14d (1.78±0.25 vs. 1.33±0.02; p=0.01) and 28d (3.25±0.53 vs. 2.10±0.18; p=0.09) post-injury, highlighting a prolonged M1-like phenotype after open fracture (i.e., OST+VML). Gene expression analysis of M1 (CCR7 and iNOS) and M2 (ARG1, CD163, and MRC1) markers revealed a mixed M1/M2 response at 3 and 14 d post-trauma (Figure 4F). Collectively, these data show elevated and mixed recruitment of M1- and M2-like macrophages to TA muscle through 28d in animals that underwent OST+VML when compared to simple fracture.

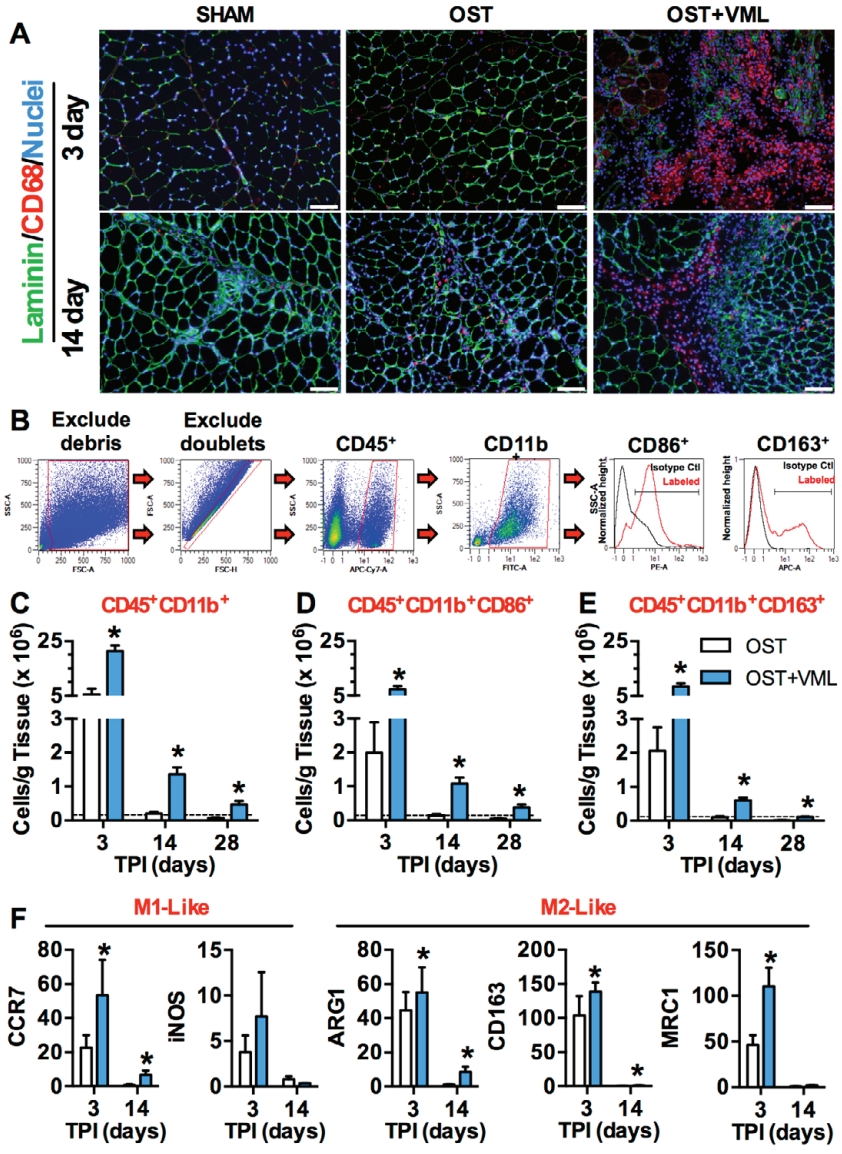

Figure 4. Heightened and prolonged recruitment of innate immune cells displaying mixed M/M2 phenotype within VML injured muscle. The TA muscle was isolated from OST, OST+VML, and specified control groups at indicated times post-injury (TPI) for A) immunofluorescence, B-E) flow cytometric, and F) transcriptional analyses. A) For immunofluorescence analysis tissue sections were stained for laminin, CD68, and nuclei (DAPI); n=4 per group. Scale bars=50 μm. B) For flow cytometric analysis, the middle third of the TA muscle that contains the defect and neighboring area was collected, digested, and cellular content isolated. Muscle-derived cells were labeled with antibodies to identify myeloid cells and analyzed by flow cytometry. To identify pro- and anti-inflammatory myeloid cells, populations were initially gated (red polygon) to exclude cell debris and doublets. Selected single cell populations were gated based on CD45 expression, followed by CD11b to identify myeloid cells. Pro- and anti-inflammatory myeloid cells were subsequently gated (black bar) based on their expression of CD86 or CD163, respectively. Gates were established by fluorescence-minus-one plus isotype controls. Relative cell numbers of C) $CD45^+CD11b^+$ myeloid cells, D) $CD45^+CD11b^+CD86^+$ pro-inflammatory myeloid cells, and E) $CD45^+CD11b^+CD163^+$ anti-inflammatory myeloid cells were determined. Dashed-lines represent average cell numbers detected within contralateral control tissue. Data are normalized per gram of tissue and presented as mean ± SEM. n=4 per group. *P<0.05 versus OST group. (F) Gene expression of M1 (*CCR7* and *iNOS*) and (F) M2-like (*ARG1*, *CD163*, and *MRC1*) macrophage markers were determined in TA muscle was isolated from OST and OST+VML groups at 3 and 14 days post-trauma by qPCR. Tissue isolated from contralateral TA muscle was used to normalize data. Data are presented as mean ± SEM. *P<0.05 versus OST group.

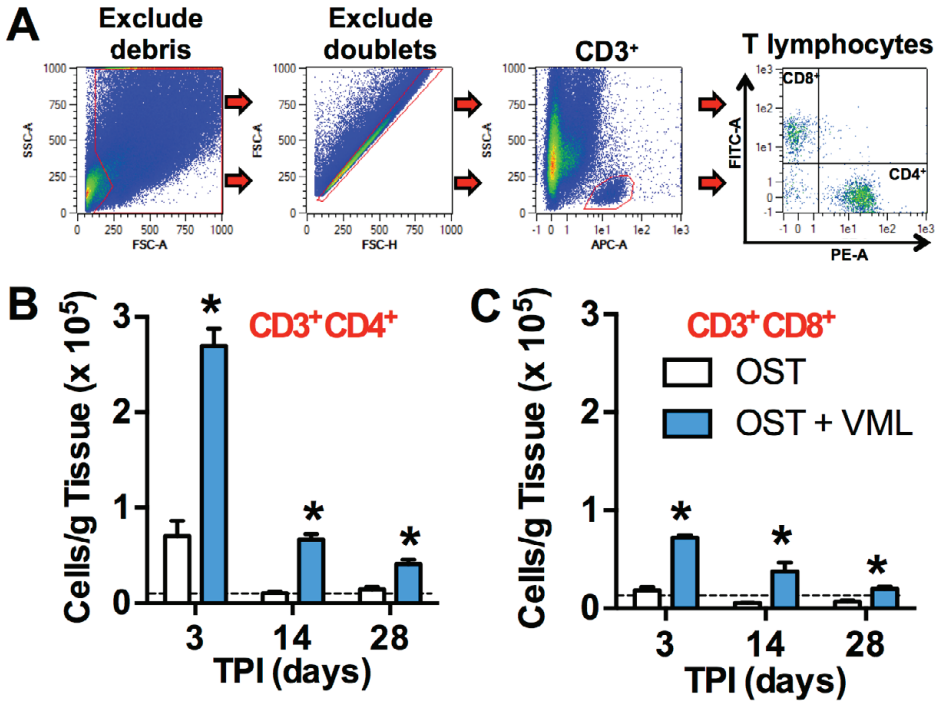

Figure 5. VML injury triggers increased recruitment of T helper and cytotoxic lymphocytes to muscle defect region. The TA muscle was isolated from OST, OST+VML, and specified control groups at indicated times points for flow cytometric analysis. A) To identify T lymphocytes (red polygon), samples were gated to exclude debris and doublets (as previously described), followed by gating for CD3 expression. $CD3^+$ cells were gated based on CD4 and CD8α expression to identify T helper and cytotoxic lymphocytes, respectively. Cells were analyzed by flow cytometry for B) $CD3^+CD4^+$ and C) $CD3^+CD8^+$ expression. Dashed-lines represent average cell numbers detected within contralateral control tissue. Data are normalized per gram of tissue and presented as mean ± SEM. n=4 per group. *P<0.05 versus OST group.

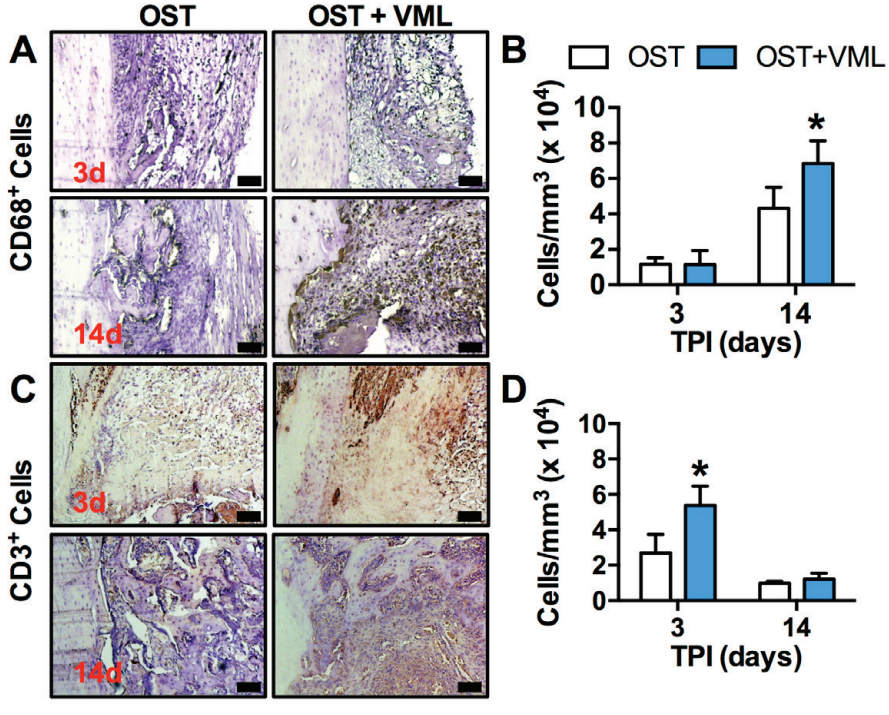

Figure 6. VML injury directly influences immune responses in the adjacent fracture callus. Affected tibiae from OST and OST+VML groups were harvested 3 and 14d post-injury for immunohistological analysis of $CD68^+$ macrophage and $CD3^+$ T-lymphocyte infiltration in the fracture callus. A & C) Representative images from the callus region for each group are presented. Scale bars=100 μm. (B & D) The number of $CD68^+$ and $CD3^+$ cells present in the callus was quantified from immunohistological sections. *p<0.05 vs. OST & OST+VML within the respective time point. Values are means ± SEM; n=3 per group.

Table 3. Transcriptional fold changes of innate and adaptive genes following OST and OST+VML injuries.

INNATE IMMUNE RESPONSE			
Pattern Recognition Receptors (PRRs) and Co-receptors			
Gene	**OST**	**OST+VML**	**p-value**
CD14	53.27±7.99	101.41±18.76	0.08
DDX58 (RIG-1)	**3.65±0.57**	**8.16±0.97**	**0.001**
NOD2	11.14±1.25	29.9±10.14	0.14
TLR1	**59.27±10.39**	**114.15±15.9**	**0.04**
TLR2	**92.39±11.39**	**227.31±18.77**	**0.004**
TLR3	0.86±0.12	0.99±0.15	0.56
TLR4	**7.61±0.38**	**12.78±0.06**	**0.0002**
TLR5	9.72±0.47	11.73±1.04	0.15
TLR6	**4.9±0.3**	**9.59±0.94**	**0.01**
TLR7	12.02±1.66	17.66±1.79	0.08
TLR9	2.88±0.08	4.81±1.27	0.2
Signaling Molecules and Transcription Factors			
Gene	**OST**	**OST+VML**	**p-value**
IRAK1	**4.19±0.23**	**5.69±0.34**	**0.02**
IRF-3	3.21±0.31	5.22±0.7	0.06
IRF-7	**2.8±0.22**	**6.7±1.12**	**0.03**
Jak2	**4.39±0.34**	**7.06±0.61**	**0.02**
Jun	2.14±0.91	1.87±0.14	0.78
Mapk1	1.71±0.55	2.09±0.14	0.54
Mapk3	3.12±0.2	6.2±1.38	0.09
Mapk8	3.43±0.26	3.03±0.3	0.37
Mapk14	1.21±0.16	1.16±0.17	0.85
MYD88	**12.97±0.99**	**25.71±2.9**	**0.01**
NFKB1	**3.22±0.29**	**6.13±0.5**	**0.01**
NFKBIA	**1.28±0.11**	**2.02±0.03**	**0.003**
Stat1	4.19±0.64	5.06±0.63	0.39
Stat4	2.41±0.76	4.26±0.82	0.17
Stat3	19.58±1.87	25.49±3.3	0.19
Stat6	**15.08±2.3**	**33.42±5.87**	**0.04**
TRAF6	**2.14±0.04**	**3.19±0.04**	**0.0001**
Cytokine/chemokine and Related Receptors			
Gene	**OST**	**OST+VML**	**p-value**
CCL12	33.26±10.22	47.74±7.9	0.32
CCR5	36.94±5.72	51.64±7.63	0.2
CCL3	2.4±0.85	11.85±5.04	0.14
CCL5 (RANTES)	1.39±0.21	1.18±0.09	0.42
CSF2	7.28±2.36	4.64±0.86	0.35
CXCL10	2.27±0.69	4.54±1.13	0.16
Ifngr1	**24.94±3.74**	**51.63±6.2**	**0.02**
IL1A	0.36±0.05	1.03±0.28	0.08
IL1R1	**9.18±0.66**	**22.45±1.08**	**0.0005**
IL6	**142.3±24.7**	**278.99±36.59**	**0.04**
CXCR3	2.33±0.57	2.28±0.97	0.97
IFNAR1	**0.68±0.21**	**1.32±0.09**	**0.05**
TNF	7.06±2.88	20.43±5.84	0.11
Acute-phase Response			
Gene	**OST**	**OST+VML**	**p-value**
C3	17.65±0.68	32.65±11.89	0.28
C5AR1	**21.38±4.41**	**68.65±10.9**	**0.02**
CAMP	4.62±2.69	19.21±15.5	0.41
CRP	2.55±0.41	1.58±0.36	0.15
LBP	21.97±2.69	14.79±1.91	0.09
Inflammasome			
Gene	**OST**	**OST+VML**	**p-value**
NLRP3	**15.11±0.87**	**33.02±0.3**	**0.00004**
IL1B	9.27±1.22	35.3±15.19	0.16
IL18	43.56±15.87	72.93±2.29	0.14
Casp1	2.42±0.01	3.97±0.74	0.1
Casp8	3.09±0.04	4±0.35	0.06
Unclassified			
Gene	**OST**	**OST+VML**	**p-value**
MX2	1.36±0.48	2.7±0.66	0.18
ITGAM (CD11b)	**89.12±18.99**	**205.71±8.14**	**0.005**
Lyz2	69.25±21.81	113.48±25.62	0.26
SLC11A1	**34.37±13.99**	**129.43±24.34**	**0.03**
MPO	3.72±3.32	53.39±48.03	0.36
Faslg	**0.95±0.12**	**2.02±0.15**	**0.01**
ADAPTIVE IMMUNE RESPONSE			
T lymphocytes - Activation and Adhesion Molecules			
Gene	**OST**	**OST+VML**	**p-value**
CD1D1	0.39±0.02	0.32±0.07	0.44
CD4	19.16±2.27	27.8±2.67	0.07
CD40	**7.22±0.29**	**16.55±2.51**	**0.02**
CD40LG	3.18±0.97	3.37±1.24	0.91
CD8A	**28.43±4.33**	**116.96±19.67**	**0.01**
CD80	**11.33±1.16**	**20.6±1.67**	**0.01**
CD86	28.24±2.73	50.37±18.06	0.29
ICAM1	**5.39±0.84**	**10.04±0.37**	**0.01**
IL2	119.51±88.48	63.96±23.72	0.58
IL23A	0.9±0.37	0.6±0.05	0.47
T lymphocyte Phenotype - Th1/Th2/Th17/Treg			
Gene	**OST**	**OST+VML**	**p-value**
CCR6	5.82±0.66	10.16±2.94	0.22
Foxp3	0.43±0.04	0.73±0.1	0.06
GATA3	0.06±0.01	0.04±0.02	0.4
IFN-g	6.19±2.86	2.79±1.45	0.35
IL4	0.31±0.03	0.24±0.11	0.61
IL10	0.49±0.14	0.67±0.03	0.27
IL13	0.27±0.08	0.29±0.11	0.86
RORC	**0.28±0.05**	**0.1±0.02**	**0.04**
Tbx21 (Tbet)	0.82±0.11	0.83±0.24	0.97

BOLD $p<0.05$, Student's t-test of OST vs. OST+VML;
Values are means ± SEM.

Complex musculoskeletal injury triggers increased recruitment of T helper and cytotoxic lymphocytes in adjacent soft tissue

The role of the adaptive immune response in sterile wound healing is an active area of research[28-30]. While animals that lack functional B and T lymphocytes display improved fracture healing[31], indicating an inhibitory response in bone regeneration, in skeletal muscle the adaptive immune response appears to be beneficial to regeneration in healthy mice but detrimental in dystrophic mice[32]. Flow cytometric analysis was carried out on cells isolated from the TA muscle, which were gated for $CD3^+$ T lymphocytes followed by $CD4^+$ and $CD8^+$ T lymphocyte markers (Figure 5A). At 3, 14, and 28d following trauma, $CD3^+CD4^+$ T lymphocytes were 3.83, 6.35, and 2.85-times higher, respectively, in OST+VML than OST muscles. At the same time points, $CD3^+CD8^+$ T lymphocytes were 3.95, 6.56, and 2.91-times higher, respectively, in the VML defect region of the OST+VML group compared to the OST group (Figures 5B&C). The OST+VML group displayed $CD3^+CD4^+$/$CD3^+CD8^+$ ratios (mean ±SEM) of 3.79±0.28, 2.02±0.42, and 2.11±0.28 at 3, 14, and 28d post-trauma, respectively. These ratios were similar compared to the OST group and indicate that initially $CD4^+$ T cells comprise a larger portion of the T lymphocyte population, but at later time points there is a progressive increase in the proportion of $CD8^+$ T cells recruited to the site of injury. Altogether open fracture promoted a heightened and prolonged innate and adaptive inflammatory response through the initial 28d post-injury.

Macrophage and T-lymphocyte recruitment to fracture callus is exacerbated by muscle trauma

The immune response to traumatized bone is crucial to regeneration, but can be deleterious if unbalanced or temporally disrupted[33]. Within the callus region, $CD68^+$ macrophages were similar among all groups 3d post-injury, but were significantly elevated 14d post-injury in non-repaired OST+VML tibia (Figures 4A&C). Meanwhile, $CD3^+$ cells were significantly elevated 3d post-injury after OST+VML, but were similar among all groups 14d post-injury (Figures 4B&D). These findings suggest that heightened inflammation within VML injured muscle directly influences immune cell infiltration within the adjacent fracture callus.

Discussion

The immune response to isolated injuries of muscle or bone is known to play a fundamental role in their regeneration[19,34]. In the context of complex fractures, investigations of the cellular components and dynamics of the ensuing inflammatory response have almost completely focused on the fracture site, with very little attention given to the surrounding traumatized musculature. Yet, the incidence of delayed and non-union rates is greatest in fracture cases that present complex injuries that often involve significant trauma or loss of surrounding muscle tissue[10,21]. Moreover, sterile "open fracture" studies in animal models unequivocally demonstrate that targeted irrecoverable muscle injury (i.e., volumetric muscle loss) or whole muscle ablation delays fracture healing via mechanisms unrelated to revascularization[11-15,35]. The current study corroborates with these earlier findings, demonstrating that TA muscle VML injury impaired fractured tibia healing in the otherwise healthy male Lewis rat. We observed heightened and prolonged myeloid and lymphocyte infiltration with the VML injured tissue and the adjacent tibia fracture callus, making it plausible that the VML injury triggered a dysregulated immune response that impaired fracture healing. These findings are in line with other conditions in which comorbid heightened inflammation is associated with impaired fracture healing[16-20,24]. The current findings therefore broadly identify the immune response to traumatized muscle, particularly VML injury, as a potential therapeutic target for advancement of open fracture orthopaedic care. These initial findings are significant because current clinical practice lacks targeted therapeutics for the systemic or local impact of traumatized skeletal muscle inflammation on musculoskeletal healing.

Volumetric muscle loss presents distinct injury characteristics that challenge mammalian skeletal muscle regeneration. Prolonged outcomes of VML include extensive fibrosis and chronic losses of muscle fibers, strength, and joint range of motion[3,5,6]. In contrast, other forms of muscle trauma in rodent models, such as eccentric-, crush-, freeze-, and toxin-induced injuries typically endogenously regenerate and fully recover muscle strength[26,36-38]. Regeneration among these recoverable injuries is partly modulated by the amplitude and dynamics of a predominantly innate immune response[34,39-42]. As an example, the osteotomy-only group presented muscle injury (likely caused by surgery) that regenerated in tandem with a typical canonical immune response, which has been characterized for recoverable eccentric and freeze injury[34,43]. Comparatively, VML injury (≈20% loss of TA muscle) incited an amplifed, prolonged, and progressively pro-inflammatory innate and adaptive immune response. It is possible that the inflammatory response following VML injury was triggered by a heightened release of endogenous danger-associated molecular patterns (DAMPS) from damaged muscle fibers[44], which are recognized by TLRs and the inflammasome and initiate cell signaling pathways that drive inflammatory responses that include the production of proinflammatory cytokines. In support, TA muscle transcript levels for several PRRs (TLR2 and TLR4), the inflammasome (NLRP3) and pro-inflammatory cytokines (IL-1, IL-6 and TNF-α) were elevated in VML injured compared to canonically healing muscle in osteotomy-only rats. Given that other recoverable muscle injuries, such as crush and ischemia-reperfusion[13,45], have not impaired fracture healing, it would appear either the sheer magnitude or composition of the immune response to VML injury is a primary determinant of musculoskeletal healing.

The cellular immune response to VML overwhelmingly consisted of macrophages, which has been highly characterized in

wound healing and shown to play phenotype-specific roles[46]. Classically activated, proinflammatory M1 macrophages directly facilitate wound repair by participating in the initial inflammatory response as debris/cell clearing phagocytes, produce reactive oxygen species (ROS) and proinflammatory cytokines (IL-1, IL-6, and TNF-α), and support a proinflammatory T helper cell phenotype (Th1). The alternative phenotype (M2) contributes to wound resolution by production of anti-inflammatory molecules (IL-4, IL-10, IL-13, IL-1R antagonist, decoy IL-1 receptor type II) and growth factors (VEGF, TGF-β, and IGF-1) and supports an anti-inflammatory T helper 2 (Th2) phenotype[46,47]. Temporal macrophage polarization is critical for successful wound healing, wherein prolonged M1 or early M2 responses result in poor regenerative outcomes. In addition, *in vivo* phenotypes are more diverse than general M1/M2 phenotypes and likely influenced by the type and/or level of injury. For example, following skeletal muscle laceration mice presented early transcriptional upregulation and macrophage surface marker expression were indicative of a mixed M1/M2 phenotype, suggesting severe muscle injury does not trigger canonical macrophage polarization[48]. Our data are in agreement in that complex musculoskeletal trauma involving VML injury does not trigger canonical polarization, as we also observed a mixed M1/M2 phenotype through day 28 based on CD86 (M1) and CD163 (M2) markers. We speculate that the inability to properly polarize local macrophages to the required phenotypes at the required times or extending presence of M1 macrophages impairs complex musculoskeletal healing partly by extending the inflammatory phase and delaying the repair and remodeling phases of bone healing. As support, Grundnes and Reikeraas showed that fracture healing was impaired following local macrophage activation with glucan, a proinflammatory molecule[49].

While the macrophage response to muscle injuries is well-studied, the T cell response is poorly characterized. We observed that VML injury induced an amplified and prolonged recruitment of $CD4^+$ and $CD8^+$ T lymphocytes within the traumatized musculature, as well as elevated gene expression of co-stimulatory molecules required for lymphocyte activation and infiltration. It is unknown if this response is non-specific (inflammatory) or antigen-specific. In sterile recoverable muscle injuries, antigen specific $CD8^+$ T cell responses are promptly regulated[50], although it is possible that a severe or persistent injury may incite an antigen-based $CD8^+$ T cell response[34]. In other muscle-based pathologies including polymyositis and Duchenne muscular dystrophy, there is marked, prolonged T lymphocyte infiltration and activity, raising the potential that VML injury possesses characteristics akin to a myopathic condition[34,51]. Notably, VML injury also resulted in elevated T lymphocytes in the adjacent fracture callus, which has previously been associated with impaired fracture healing[31]. For example, $CD8^+$ T cell recruitment and terminal differentiation in fracture hematomas are associated with impaired healing[28,52], while depletion improved bone repair[53]. Impaired musculoskeletal healing may be due to modulation of various activation and effector functions of $CD8^+$ T cells including polarization (cytokine production), cell lysis via perforin and granzyme B, and cellular interactions. We therefore hypothesize that VML injury prompts a $CD8^+$ T cell response that impairs musculoskeletal regeneration that may be effectively targeted by immunomodulatory therapies.

Similar to $CD8^+$ T cells, we show $CD4^+$ T cells were recruited at increased numbers through 28 d following OST+VML. Although depletion studies in normal fracture healing suggest a beneficial effect[53], literature also suggests that during pathologies (arthritis, infection, cancer) $CD4^+$ T lymphocytes are detrimental in bone repair processes[54]. Whether $CD4^+$ T cells are beneficial or detrimental to fracture repair likely depends on the magnitude and duration of T cell recruitment, T helper cell polarization (Th1/Th2/Th17) and production of pro- or anti-inflammatory cytokines. For example, T helper polarization impacts osteoblasts and osteoclasts and influence cellular activation and function, all which can indirectly uncouple the bone repair process[54]. Lymphocytes can also directly impair fracture healing by the release of soluble factors including RANKL, which activate osteoclasts as well as direct cell-to-cell (CD40-CD40L) contact of stromal cells, which impact RANKL and OPG levels[54]. Impaired healing could also be tied in to the recruitment, or lack of T regulatory cells (Tregs). Tregs make up a small percentage of $CD4^+$ T lymphocytes and modulate the immune response by anti-inflammatory mechanisms (IL-10, TGF-β, direct cell-to-cell interactions). Recently, Tregs have been shown to infiltrate injured muscle and secrete amphiregulin, which was required for successful muscle repair[55]. Additionally, Tregs modulate regeneration following recoverable toxin injury via a putative interaction with resident satellite cells[29]. We found transcriptional expression of Foxp3, the master regulator of Treg development and function, was not significantly upregulated in injured muscle following complex musculoskeletal injury. These differences suggest Treg induction/recruitment and amphiregulin production may be low following complex musculoskeletal injury and partly explain impaired healing. It is essential that future studies are carried out to evaluate the impact of modulating T lymphocyte recruitment, activation, polarization, and secretion of factors (e.g., amphiregulin) in both traumatized muscle and bone to favor tissue repair.

The current data provide the most extensive characterization of the immune response to VML injury to date. As predicted by the irrecoverable nature of VML, the ensuing immune response deviates from that described for canonical muscle regeneration. Notably, VML presents a prolonged mixed M1/M2 response and heightened lymphocyte infiltration that resembles pathological muscle tissue. The data indicate that VML results in heightened macrophage and lymphocyte infiltration within the fracture callus of adjacently fractured bone and impairs fracture healing. It is important to note that this rat model of open fracture did not include blunt trauma, and it is likely that the magnitude and temporal characteristics of the dysregulated immune response to VML are further exacerbated in the clinic[56]. We posit that VML presents various targets that may be targeted by immunomodulatory therapies for the improvement of bone and muscle regeneration following complex musculoskeletal injuries.

Acknowledgements

This work was supported by the Combat Casualty Care Research Program, Medical Research and Materiel Command (BTC) and the Orthopaedic Trauma Association (BTC & TOM). This work was performed as part of a service obligation to the NIH-LRP (BTC). BJH and CLW were post-doctoral fellows through the National Academy of Sciences during a portion of these studies. We thank Dr. Lisa Ji and Ms. Monica Jalomo for their technical assistance.

References

1. MacKenzie EJ, Bosse MJ. Factors influencing outcome following limb-threatening lower limb trauma: lessons learned from the Lower Extremity Assessment Project (LEAP). J Am Acad Orthop Surg 2006;14:S205-10.
2. Doukas WC, Hayda RA, Frisch HM, et al. The Military Extremity Trauma Amputation/Limb Salvage (METALS) study: outcomes of amputation versus limb salvage following major lower-extremity trauma. J Bone Joint Surg Am 2013;95:138-45.
3. Corona BT, Garg K, Ward CL, McDaniel JS, Walters TJ, Rathbone CR. Autologous minced muscle grafts: a tissue engineering therapy for the volumetric loss of skeletal muscle. Am J Physiol Cell Physiol 2013;305:C761-75.
4. Garg K, Corona BT, Walters TJ. Losartan administration reduces fibrosis but hinders functional recovery after volumetric muscle loss injury. J Appl Physiol (1985) 2014;117:1120-31.
5. Garg K, Ward CL, Hurtgen BJ, et al. Volumetric muscle loss: persistent functional deficits beyond frank loss of tissue. J Orthop Res 2015;33:40-6.
6. Garg K, Ward CL, Rathbone CR, Corona BT. Transplantation of devitalized muscle scaffolds is insufficient for appreciable de novo muscle fiber regeneration after volumetric muscle loss injury. Cell Tissue Res 2014;358:857-73.
7. Mase VJ Jr, Hsu JR, Wolf SE, et al. Clinical application of an acellular biologic scaffold for surgical repair of a large, traumatic quadriceps femoris muscle defect. Orthopedics 2010;33:511.
8. Corona BT, Rivera JC, Owens JG, Wenke JC, Rathbone CR. Volumetric muscle loss leads to permanent disability following extremity trauma. J Rehabil Res Dev 2015;52:785-92.
9. Rivera JC, Corona BT. Muscle-related Disability Following Combat Injury Increases With Time. US Army Med Dep J 2016:30-4.
10. Papakostidis C, Kanakaris NK, Pretel J, Faour O, Morell DJ, Giannoudis PV. Prevalence of complications of open tibial shaft fractures stratified as per the Gustilo-Anderson classification. Injury 2011;42:1408-15.
11. Utvag SE, Grundnes O, Reikeras O. Early muscle-periosteal lesion inhibits fracture healing in rats. Acta Orthop Scand 1999;70:62-6.
12. Utvag SE, Iversen KB, Grundnes O, Reikeras O. Poor muscle coverage delays fracture healing in rats. Acta Orthop Scand 2002;73:471-4.
13. Utvag SE, Grundnes O, Rindal DB, Reikeras O. Influence of extensive muscle injury on fracture healing in rat tibia. J Orthop Trauma 2003;17:430-5.
14. Willett NJ, Li MT, Uhrig BA, et al. Attenuated human bone morphogenetic protein-2-mediated bone regeneration in a rat model of composite bone and muscle injury. Tissue Eng Part C Methods 2013;19:316-25.
15. Harry LE, Sandison A, Paleolog EM, et al. Comparison of the healing of open tibial fractures covered with either muscle or fasciocutaneous tissue in a murine model. J Orthop Res 2008;26:1238-44.
16. Wong SC, Catto-Smith AG, Zacharin M. Pathological fractures in paediatric patients with inflammatory bowel disease. Eur J Pediatr 2014;173:141-51.
17. Loder RT. The influence of diabetes mellitus on the healing of closed fractures. Clin Orthop Relat Res 1988:210-6.
18. Stromqvist B. Hip fracture in rheumatoid arthritis. Acta Orthop Scand 1984;55:624-8.
19. Claes L, Recknagel S, Ignatius A. Fracture healing under healthy and inflammatory conditions. Nat Rev Rheumatol 2012;8:133-43.
20. Recknagel S, Bindl R, Kurz J, et al. Experimental blunt chest trauma impairs fracture healing in rats. J Orthop Res 2011;29:734-9.
21. Bhandari M, Tornetta P, 3rd, Sprague S, et al. Predictors of reoperation following operative management of fractures of the tibial shaft. J Orthop Trauma 2003;17:353-61.
22. Novotny SA, Warren GL, Lin AS, Guldberg RE, Baltgalvis KA, Lowe DA. Prednisolone treatment and restricted physical activity further compromise bone of mdx mice. J Musculoskelet Neuronal Interact 2012;12:16-23.
23. Mojumdar K, Liang F, Giordano C, et al. Inflammatory monocytes promote progression of Duchenne muscular dystrophy and can be therapeutically targeted via CCR2. EMBO Mol Med 2014;6:1476-92.
24. Abou-Khalil R, Yang F, Mortreux M, et al. Delayed bone regeneration is linked to chronic inflammation in murine muscular dystrophy. J Bone Miner Res 2014;29:304-15.
25. Criswell TL, Corona BT, Ward CL, et al. Compression-induced muscle injury in rats that mimics compartment syndrome in humans. Am J Pathol 2012;180:787-97.
26. Lowe DA, Warren GL, Ingalls CP, Boorstein DB, Armstrong RB. Muscle function and protein metabolism after initiation of eccentric contraction-induced injury. J Appl Physiol (1985) 1995;79:1260-70.
27. Corona BT, Wu X, Ward CL, McDaniel JS, Rathbone CR, Walters TJ. The promotion of a functional fibrosis in skeletal muscle with volumetric muscle loss injury following the transplantation of muscle-ECM. Biomaterials 2013;34:3324-35.
28. Reinke S, Geissler S, Taylor WR, et al. Terminally differentiated CD8(+) T cells negatively affect bone regeneration in humans. Sci Transl Med 2013;5:177ra36.

29. Castiglioni A, Corna G, Rigamonti E, et al. FOXP3+ T Cells Recruited to Sites of Sterile Skeletal Muscle Injury Regulate the Fate of Satellite Cells and Guide Effective Tissue Regeneration. PLoS One 2015;10:e0128094.
30. Schlundt C, Schell H, Goodman SB, Vunjak-Novakovic G, Duda GN, Schmidt-Bleek K. Immune modulation as a therapeutic strategy in bone regeneration. J Exp Orthop 2015;2:1.
31. Toben D, Schroeder I, El Khassawna T, et al. Fracture healing is accelerated in the absence of the adaptive immune system. J Bone Miner Res 2011;26:113-24.
32. Farini A, Meregalli M, Belicchi M, et al. T and B lymphocyte depletion has a marked effect on the fibrosis of dystrophic skeletal muscles in the scid/mdx mouse. J Pathol 2007;213:229-38.
33. Einhorn TA, Gerstenfeld LC. Fracture healing: mechanisms and interventions. Nat Rev Rheumatol 2015;11:45-54.
34. Tidball JG, Villalta SA. Regulatory interactions between muscle and the immune system during muscle regeneration. Am J Physiol Regul Integr Comp Physiol 2010; 298:R1173-87.
35. Harry LE, Sandison A, Pearse MF, Paleolog EM, Nanchahal J. Comparison of the vascularity of fasciocutaneous tissue and muscle for coverage of open tibial fractures. Plast Reconstr Surg 2009;124:1211-9.
36. Plant DR, Colarossi FE, Lynch GS. Notexin causes greater myotoxic damage and slower functional repair in mouse skeletal muscles than bupivacaine. Muscle Nerve 2006;34:577-85.
37. Stratos I, Graff J, Rotter R, Mittlmeier T, Vollmar B. Open blunt crush injury of different severity determines nature and extent of local tissue regeneration and repair. J Orthop Res 2010;28:950-7.
38. Warren GL, Hulderman T, Mishra D, et al. Chemokine receptor CCR2 involvement in skeletal muscle regeneration. FASEB J 2005;19:413-5.
39. Tidball JG, Dorshkind K, Wehling-Henricks M. Shared signaling systems in myeloid cell-mediated muscle regeneration. Development 2014;141:1184-96.
40. Ishikawa M, Ito H, Kitaori T, et al. MCP/CCR2 signaling is essential for recruitment of mesenchymal progenitor cells during the early phase of fracture healing. PLoS One 2014;9:e104954.
41. Kamimura M, Mori Y, Sugahara-Tobinai A, Takai T, Itoi E. Impaired Fracture Healing Caused by Deficiency of the Immunoreceptor Adaptor Protein DAP12. PLoS One 2015;10:e0128210.
42. Aguilar CA, Shcherbina A, Ricke DO, et al. *In vivo* Monitoring of Transcriptional Dynamics After Lower-Limb Muscle Injury Enables Quantitative Classification of Healing. Sci Rep 2015;5:13885.
43. Summan M, McKinstry M, Warren GL, et al. Inflammatory mediators and skeletal muscle injury: a DNA microarray analysis. J Interferon Cytokine Res 2003;23:237-45.
44. Bianchi ME. DAMPs, PAMPs and alarmins: all we need to know about danger. J Leukoc Biol 2007;81:1-5.
45. Kase T, Skjeldal S, Nordsletten L, Reikeras O. Healing of tibial fractures is not impaired after acute hindlimb ischemia in rats. Arch Orthop Trauma Surg 1998;117:273-6.
46. Koh TJ, DiPietro LA. Inflammation and wound healing: the role of the macrophage. Expert Rev Mol Med 2011;13:e23.
47. Laskin DL, Sunil VR, Gardner CR, Laskin JD. Macrophages and tissue injury: agents of defense or destruction? Annu Rev Pharmacol Toxicol 2011;51:267-88.
48. Novak ML, Weinheimer-Haus EM, Koh TJ. Macrophage activation and skeletal muscle healing following traumatic injury. J Pathol 2014;232:344-55.
49. Grundnes O, Reikeraas O. Effects of macrophage activation on bone healing. J Orthop Sci 2000;5:243-7.
50. Liao H, Franck E, Freret M, et al. Myoinjury transiently activates muscle antigen-specific CD8+ T cells in lymph nodes in a mouse model. Arthritis Rheum 2012;64:3441-51.
51. Rigamonti E, Zordan P, Sciorati C, Rovere-Querini P, Brunelli S. Macrophage plasticity in skeletal muscle repair. Biomed Res Int 2014;2014:560629.
52. Schmidt-Bleek K, Schell H, Schulz N, et al. Inflammatory phase of bone healing initiates the regenerative healing cascade. Cell Tissue Res 2012;347:567-73.
53. Davis PA, Corless DJ, Aspinall R, Wastell C. Effect of CD4(+) and CD8(+) cell depletion on wound healing. Br J Surg 2001;88:298-304.
54. Jones D, Glimcher LH, Aliprantis AO. Osteoimmunology at the nexus of arthritis, osteoporosis, cancer, and infection. J Clin Invest 2011;121:2534-42.
55. Burzyn D, Kuswanto W, Kolodin D, et al. A special population of regulatory T cells potentiates muscle repair. Cell 2013;155:1282-95.
56. Evans KN, Forsberg JA, Potter BK, et al. Inflammatory cytokine and chemokine expression is associated with heterotopic ossification in high-energy penetrating war injuries. J Orthop Trauma 2012;26:e204-13.